CAPTURING THE SOURCE PARAMETERS CONTROLING THE HIGH-FREQUENCY GROUND MOTION

R. FAYJALOUN[1], M. CAUSSE[1], C. CORNOU[1], C. VOISIN[1], S.G. SONG[2]

[1]Univ. Grenoble Alpes, Univ. Savoie Mont Blanc, CNRS, IRD, IFSTTAR, ISTerre, 38000 Grenoble, France

[2]Earthquake Research Center, Korea Institute of Geoscience and Mineral Resources (KIGAM), 124 Gwahang-no, Yuseong-gu, Daejon 34132, Korea.

E-mail contact of main author: rose-marie.fayjaloun@univ-grenoble-alpes.fr

Abstract. During an earthquake, seismic waves carry the complexity of the rupture to the ground surface. Empirical ground motion prediction equations, calibrated by past earthquake seismic recordings, are often used to predict Peak Ground Acceleration (PGA) and its variability. However, the scarcity of near-fault recordings for large earthquakes prevents using such equations to predict near-fault PGA. Simulation of strong ground motion then offers an attractive alternative (e.g. [1]) to assess seismic hazard in near-fault if realistic scenarios of seismic rupture are provided. In order to better understand the effects of rupture parameters on surface ground motion and to capture the key source ingredients that most impact ground motion variability, we simulate ground motions produced by various M7 rupture earthquake scenarios on a vertical strike-slip fault. We compute the ground motion up to 5Hz at sites located at 5 km, 25 km and 70 km from the fault and in the far-field. The rupture parameters (rupture speed, slip, rise time) are modeled by using a statistical source model generator in which the source complexity is modeled in terms of standard deviation, spatial correlation length and correlation between source parameters, as proposed in [2]. In the far-field, we show that PGA is mainly generated by abrupt changes of the rupture propagation, that is, stopping phases at the fault boundaries or strong heterogeneities of rupture speed along the rupture. We observe that PGA is mostly controlled by the average rupture speed and the average stress drop, and to a lesser extent by the standard deviation of the rupture speed... Interestingly, correlation between source parameters and spatial correlation length do not affect average PGA and related variability significantly.

Key Words: Source Simulation, Near-fault and Far-fault PGA, Sensitivity.

1. Introduction

Earthquakes have caused, and can cause in the future, enormous loss of life, injury, destruction of property, and economic and social disorder. Determining the earthquake intensity does help developers make good decisions about where to build and what type of forces structures should withstand. Statistical analysis of strong ground motion databases helps providing quantitative estimates of expected ground-motion levels for a potential future earthquake. Due to the lack of recordings in the vicinity of faults, there is however the need to develop physics-based simulation techniques incorporating the complexity of earthquake rupture to obtain reliable near-field ground motions (e.g. [1]). The present study focuses on the relationship between the rupture process and the high-frequency ground motion (average and variability) represented by the Peak Ground Acceleration (PGA).

It is commonly claimed that the PGA is driven by the stress drop $\Delta\tau$ (e.g. [3]–[5]), which is related to the available elastic energy during the rupture process on the rupture area. The stress drop is commonly supposed to be proportional to the cube of the corner frequency f_c, determined from the Fourier amplitude spectra of the displacement ground motion, under the assumption of a ω^{-2} source model [6]. In the framework of stochastic simulations of ground motion time histories, the stress drop is then generally used to control the high-frequency level of ground motion (e.g. [7]). Using the random vibration theory, [7] obtained that $PGA \propto {f_c}^{2.4}$, leading to $PGA \propto \Delta\tau^{0.8}$ for a Brune (1970) source model. Recently, [8] pointed out the importance of considering the rupture velocity V_r in the corner frequency definition, and obtained:

$$PGA \propto \Delta\tau^{0.8} {V_r}^{2.4} \qquad (1)$$

Note that in Equation (1), $\Delta\tau$ and V_r are considered as average source properties. As such, the PGA is controlled by the corner frequency, which, in turn, depends on large-scale source parameters describing the macroscopic features of the rupture process.

On the other hand, several studies suggest that the high-frequency ground motion may be controlled by smaller-scale processes at frequencies larger than the corner frequency. Recently, [9] proposed that earthquake moment-rate functions are better fitted by a two-corner frequency spectrum model. The largest one may be associated with local-scale source parameters and controls the PGA. Which of those source processes mainly control the high-frequency ground motion remains however strongly debated. Using dynamic rupture simulations, [10] showed that strong variations of the rupture velocity are very efficient sources of high frequency radiation, especially rupture stopping phases at the fault boundaries. This is confirmed by rupture analyses using “back-projection” techniques of teleseismic high-frequency body waves (e.g. [11]). Besides, [12] claimed that PGA is directly

connected to the characteristic length of static slip asperities, small slip asperities generating larger PGA values. This contradicts [13], who showed that large asperities increase ground motion coherency and lead to higher PGA values. Furthermore, [14] claims that high-frequency ground motion is much more sensitive to the peak slip-rate than slip heterogeneities. These contradictory results shed the light on the need for further investigations on the link between the heterogeneity level of kinematic rupture parameters and high-frequency ground motion. Finally, small-scale source heterogeneities pertain seismic motion wavelengths that are difficult to model owing to uncertainties in the propagation medium. Small-scale heterogeneities remain then poorly resolved by source studies.

Based on heterogeneous spontaneous dynamic rupture simulations, several authors showed that local kinematic source parameters may not be independent but correlated (e.g., [2], [15], [16]). Such correlations may also impact the ground motion and its variability. Thus, larger correlation between source parameters may produce stronger peak ground velocities near the source [16]. Nevertheless, the level of correlation between kinematic source parameters remains poorly constrained, because it strongly depends on the friction law assumed in the dynamic simulations [17].

This study aims to identify the kinematic source parameters that mostly control the PGA and its variability, deploying numerical ground motion simulations in the frequency range [0-5 Hz]. First, we identify the mechanisms of PGA generation in homogeneous kinematic ruptures. Thenceforward, we study the PGA generated in heterogeneous kinematic ruptures. Afterwards, we run a sensibility analysis to determine the kinematic source parameters that mostly contribute to the PGA and its variability. We consider not only “large-scale” source parameters (average stress drop and average rupture velocity) but also “local-scale” parameters, that is statistical parameters controlling the level of source heterogeneity as well as the level of correlation between source parameters.

2. Mechanism of PGA generation in kinematic source models

2.1.Earthquake source model

Earthquake ruptures generate seismic waves that travel from the source to the surface and cause ground motions over a wide range of frequencies. One approach to describe the source process is the so-called kinematic approach, which consists in *a priori* prescribing the displacement discontinuity across the fault surface. The local slip-rate function needs to be specified (e.g. [18], [19]) to describe the space-time evolution of slip along the fault by means of kinematic parameters. We use the pseudo-dynamic source model developed by [2] for a rectangular fault plane. In this model, kinematic source parameters are calibrated using

suite of spontaneous heterogeneous dynamic rupture simulations. The rupture starts from the hypocenter and expands over the fault plane with a rupture speed (V_r). Each point on the fault slips as it is reached by the rupture front and thus is characterized by a final slip value (D) and a peak slip velocity (psv). In order to characterize the spatial variability of the kinematic source parameters (V_r, D and psv) over the fault area, two statistical properties are considered. First, the 1-point statistics is defined for a given fault point by the mean value (μ) and the standard deviation (σ) of the considered source parameter, considering a normal distribution. Second, the 2-point statistics is defined by the correlation lengths (a_x and a_z, representing the characteristic length of heterogeneities along-strike and along-dip, respectively) and the spatial cross-correlation, defined by the correlation coefficient (ρ) between any pair of kinematic parameters at a given point, and by a correlation function. We use a Von Karman autocorrelation function [20]. Note that our statistical model is stationary, which implies that the statistics of any parameter is constant over the fault plane.

2.2.Earthquake source parameterization

We generate rupture models equivalent to a moment magnitude **M**=7 (FIG. 1). The rupture length L=70 km and width W=14 km are derived from the $M_w - L$ scaling relationship by [21]. The mean value of the slip μ_D is then defined by: $\mu_D = \frac{M_0}{G\,L\,W}$, where M_0 is the seismic moment and G is the shear modulus. We make sure that the maximum slip does not exceed the ceiling defined by [22] as a function of magnitude. The average stress drop $\Delta\tau$ is expressed as:

$$\Delta\tau = C\frac{\mu_D}{\sqrt{L * W}} \qquad (2)$$

where C is a shape factor with a value close to 1 [23]. The average value of the rupture speed μ_{Vr} is chosen in the range of values commonly reported by source studies [24]. We then assume that $\mu_{Vr} = 0.8V_s$, where V_s is the shear wave speed. The mean value of the psv is chosen from the database of spontaneous dynamic rupture simulations developed by [2]. The slip duration, also called rise time T_{rise}, is calculated as a function of the peak slip velocity psv and the slip value D, for a Yoffe slip-rate function [19]. T_{rise} is allowed to vary between 0.1 and 5s. The fault area is embedded in at 0.5 km below the surface. The spatial distribution of final slip and rupture speed are tapered so as to avoid stress singularities at the fault boundaries. Therefore, the values of the source parameters decrease to zero as they reach 20% of the fault dimension at each side, with a quarter circular taper. We fix the hypocenter position to 20% of the rupture length along the strike and 80% along the dip [25], such that the rupture propagates unilaterally.

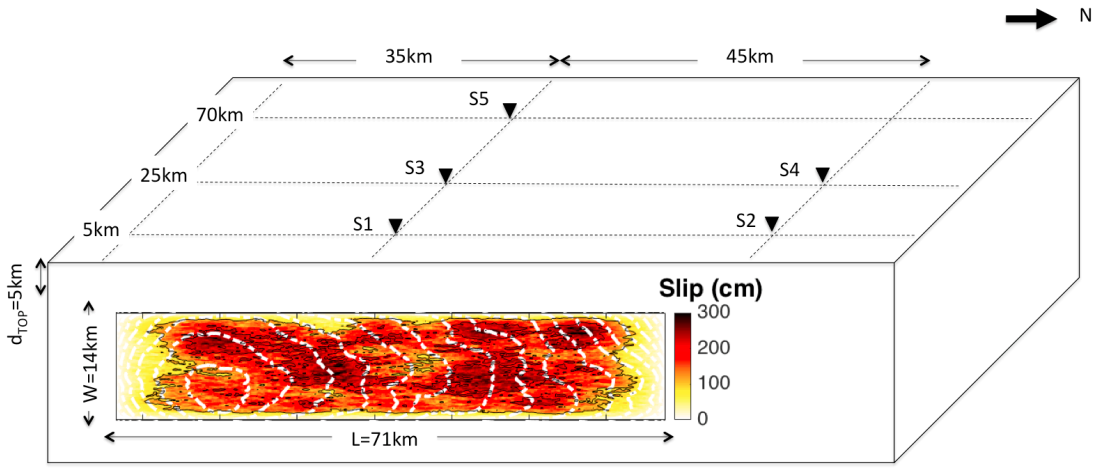

*FIG. 1. Illustration of a rupture realization on the vertical fault plane, corresponding to a **M**7 event, and location of stations S1, S2, S3, S4 and S5.*

2.3.PGA computation in the far-field approximation

The ground motion for a homogeneous elastic medium in the far-field approximation $u_{FF}(t)$ is proportional to the source time function, also called the moment rate function $\dot{M}(t)$. We use Equation (3) to compute the ground motion:

$$u_{FF}(t) = \frac{1}{4\pi\rho {V_s}^3} \times \frac{RP}{X} \times \dot{M}\left(t - \frac{X}{V_s}\right) \times exp\left(-\frac{\pi f X}{V_s Q_s}\right) \quad (3)$$

where X is the distance to the rupture, assumed equal to 100 km, ρ is the rock density (ρ=2.7g/cm^3), V_s is the shear wave speed (V_s=3.58km/s), RP is the average radiation pattern of the shear waves (according to [26], we assume RP=0.63), Q_s is the attenuation factor (we choose Q_s=220, which is a realistic value, e.g. [27]) and t and f are the time and the frequency. The attenuation of ground motion is represented by the geometrical attenuation $1/X$ and by the anelastic attenuation $exp\left(-\frac{\pi f X}{V_s\, Q_s}\right)$. We then compute PGA as the maximum absolute value of the displacement second derivative. Note that a quarter-period-cosine taper is applied to the first second of the acceleration to remove the artificial strong phase due to the sharp increase of rupture velocity at the rupture nucleation. Theoretical studies show that the rupture velocity increases smoothly during nucleation (e.g. [28]) and such initiation phases are not observed on real seismograms.

2.4.Mechanism of PGA generation for homogeneous ruptures

We start by investigating homogeneous ruptures, in order to identify the mechanisms of PGA generation in a simple rupture case. The slip, the rupture speed and the rise time are then constant along the rupture ($\sigma = 0$), except at the fault boundaries due to the applied tapering.

The parameters used for simulations are summarized in TABLE 1 (simulation A). We use the concept of isochrones to extract the part of the rupture that produces the PGA [29]. Isochrones are all the points on the fault that radiate elastic waves that arrive at a given station at the same time. In the case of the far-field approximation (Equation (3)), the isochrone at the PGA time is simply the rupture front at the PGA time (FIG. 2a, b, c).

TABLE 1: The source parameters: Mw, L, W, $\Delta\tau$, D, Vr, a_x, a_z, psv, and T_{rise} stand for the magnitude, length, width, stress drop, slip, rupture speed, spatial correlation lengths along the strike and along the dip directions, peak slip velocity and rise time, respectively. μ represents the mean value, σ is the standard deviation and ρ is the coefficient of correlation.

simulation	Mw	L (km)	W (km)	μD (cm)	Δτ (MPa)	σD/μD	μVr (km/s)	σVr/μVr	ρD-Vr	ax (km)	az (km)	μ psv (cm/s)	σ psv	ρD-psv	risT (s)	risT min	risT max	circular taper
A	7	70	14	121.69	1.28	0	3	0	-	-	-	80	0	0.8	f(D, psv)	0.1	5	L/5 ou W/5
B						0.5		0.5	0	4	2		50					
1	7	70	14	121.69	1.28	0.5	3	0.25	0	16	5	80	50	0.8	f(D, psv)	0.1	5	L/5 ou W/5
2						0.5	2.5	0.25	0	16	5							
3						1	3	0.25	0	16	5							
4						0.5	3	0.5	0	16	5							
5						0.5	3	0.25	0	4	2							
6						0.5	3	0.5	1	16	5							
7						0.5	3	0.5	-1	16	5							
8		55		154.14	1.83	0.5	3	0.25	0	16	5							

For homogeneous ruptures, we notice that ground acceleration is essentially dominated by four peaks (FIG. 2e), corresponding to the times where the rupture reaches the four fault boundaries. For the chosen rupture nucleation position and fault boundary tapering function, the stopping phase generated by the rupture arrest at the fault top is responsible for the PGA. Since the tapering function determines the sharpness of the rupture stopping, it highly controls the PGA value. Thus, increasing the tapering length for both the rupture velocity and the slip tends to decrease the PGA (FIG. 2f). In the following we explore the impact of various kinematic parameters on the PGA.

By decreasing the length of the rupture L while preserving the magnitude, we increase the stress drop $\Delta\tau$ and the slip D. Considering a decrease of L by a factor of 1.2, D and $\Delta\tau$ increases by factors of 1.2 and 1.31, respectively. According to Equation (1), PGA should then increase by a factor of ~1.24. Though the PGA remains almost unchanged. This is because Equation (1) is derived assuming a simple Brune's source model and random phases for the source spectrum [6]. PGA is then estimated using the random vibration theory and depends only on the corner frequency (that is, the overall rupture duration). Our source model also matches a Brune's source model (FIG. 2d). However PGA is not driven by the corner frequency but is rather controlled locally by the rupture stopping. And the induced stopping phases remain poorly affected by the stress drop increase.

We next analyse the effect of the rupture velocity Vr and the rise time T_{rise}. According to Equation (1), changing V_R from 3 to 3.3 km/s should increase the PGA by a factor of 1.25 (FIG. 2h). This is also the case in our simulations. But again, we note that the simulated PGA cannot be modelled using random phases but is generated by a local process. Furthermore,

reducing the T_{rise} value from 4 to 1.5 s increases the ground motion amplitude spectral level above f≈1/4=0.25 Hz (FIG. 2d), but only increases the PGA value by 15% (FIG. 2i). This implies that the PGA stopping phase is little sensitive to the width of the local slip function.

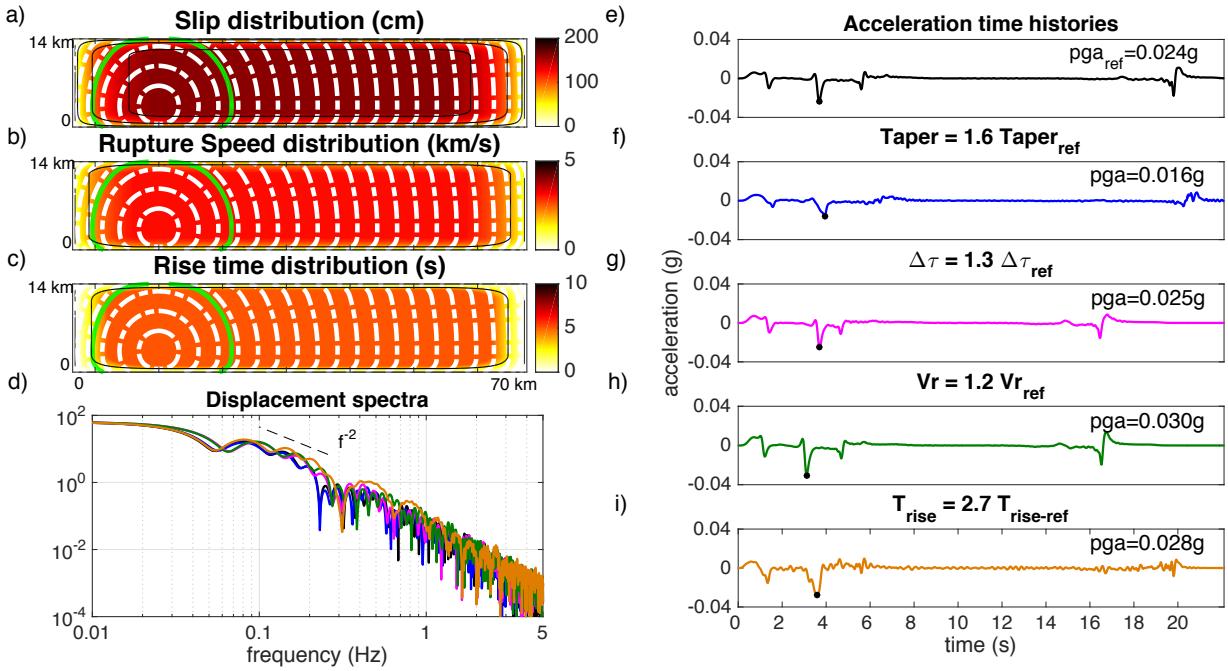

*FIG. 2. a) to c). Kinematic rupture parameters for a homogeneous rupture of a **M**7 event, with L=70km, V_r=3km/s, and T_{rise}=4s, tapered at the boundaries. The white contour lines represent the propagation time and the green contouring shows the location of the rupture front at the PGA time. d). Displacement spectra for all the scenarios presented in cases e) to i). e). Acceleration calculated using Equation (3), corresponding to the scenario shown in a to c. This acceleration is referred to as the reference case. f). Accelerogram obtained using a wider taper at the fault boundaries. g). Accelerograms due to a smaller rupture length while keeping M=7; the stress drop, calculated using Equation (2), is increased by a factor of 1.3. h). Accelerogram in case of a faster rupture speed Vr=3.3km/s. i). Accelerogram obtained for a shorter rise time of 1.5s.*

2.5.Mechanism of PGA generation for heterogeneous ruptures

FIG. 3a and 3b show two different realizations of heterogeneous ruptures with the same statistical properties of the source parameters (TABLE 1 - simulation B). These source models are associated with two different mechanisms of PGA generation. On the one hand, the PGA on FIG. 3a is induced by the rupture stopping at the top fault boundary, as observed for a homogeneous rupture. The PGA is however higher (0.04 g instead of 0.024 g) because the rupture speed is heterogeneous and gives rise to a stronger rupture speed drop in this case. On the other hand, the PGA on FIG. 3b is controlled by the large rupture speed patches located at the right edge of the rupture, resulting in an abrupt change of rupture velocity.

Thus, the position of the high rupture speed patches and their interactions with the fault boundaries seems to play an important role in the PGA generation. Note that the PGA is little sensitive to the correlation length a_x (characteristic length of rupture heterogeneities), as illustrated in FIG. 4. Moreover, it is interesting to note that the PGA sensitivity to the rise time value is much stronger than for an homogeneous rupture.

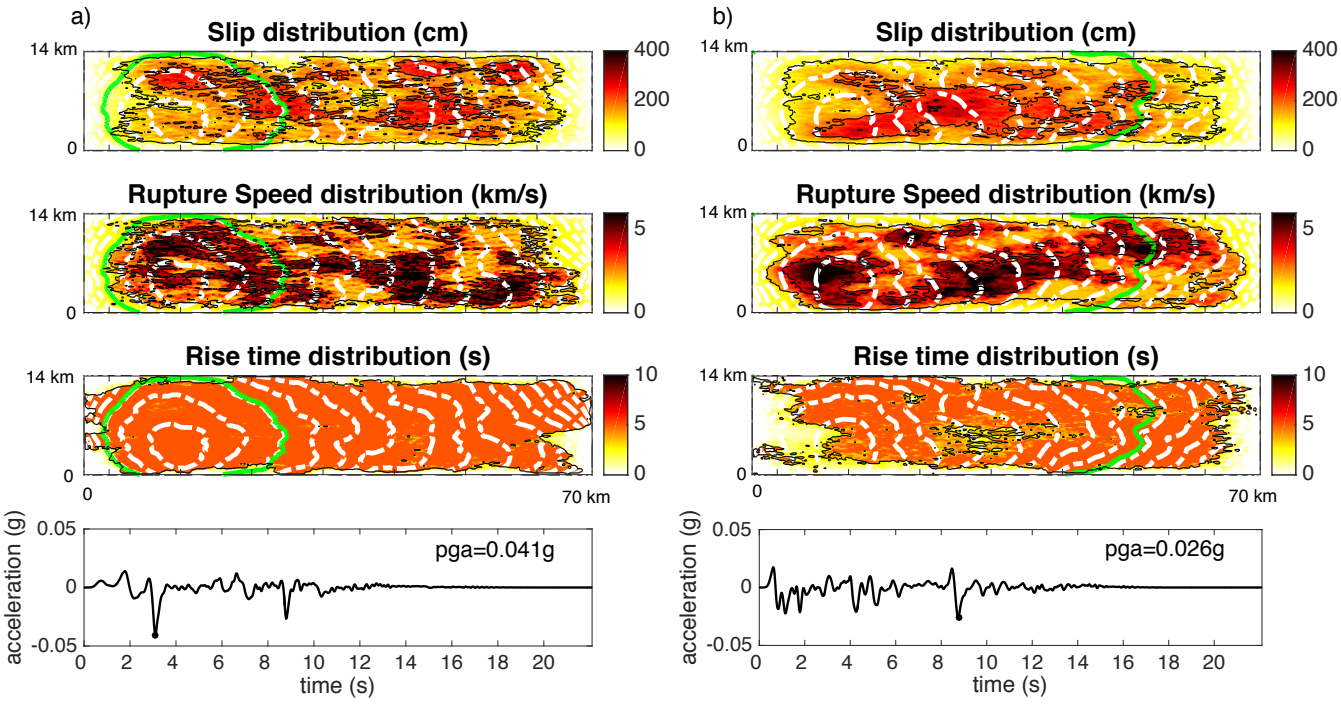

*FIG. 3. Two realizations of heterogeneous ruptures of a **M**7 event, with L=70km, V_r=3km/s, and T_{rise}=4s, tapered at the boundaries and the corresponding acceleration computed using Equation (3). The statistical parameters are* $\sigma_D = 0.5\mu_D$, $\sigma_{Vr} = 0.5\mu_{Vr}$, a_x=4km, ρ_{D-Vr}=0.

3. Sensitivity of PGA to source parameters

The above-mentioned tests illustrate some important source mechanisms involved in the PGA generation. We now aim to quantify the PGA sensitivity to the source parameters, by perturbing one parameter at a time. We still compute PGA in the far-field approximation (Equation (3)), but also for a network of near-field stations (FIG. 1). First, we investigate the sensitivity to the 1-point and 2-point statistical parameters describing the rupture heterogeneity, which are very poorly constrained (e.g. [17]). We also compute the sensitivity to large-scale source parameters (average rupture velocity and average stress drop).

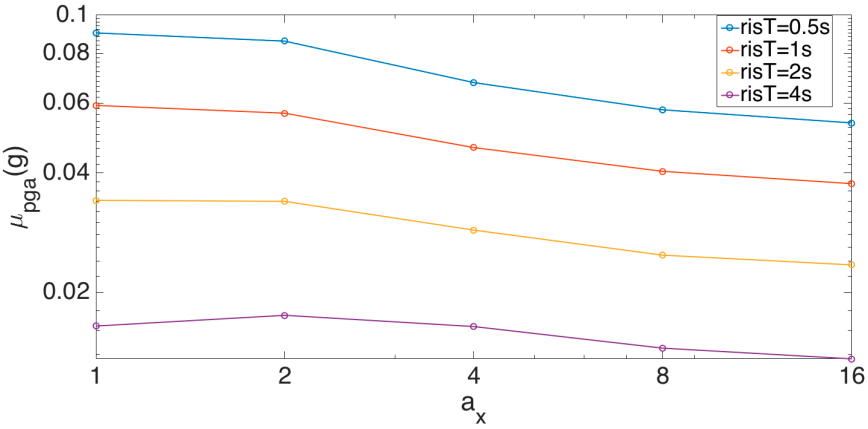

FIG. 4. Mean PGA value (over 50 rupture realizations) for different combinations of rise-time and spatial correlation length values.

3.1.Computation of near-fault PGA

We synthesize near-fault ground motions in a 1D layered medium (APPENDIX 1) for stations located at rupture distances R_{rup} of 5 km (station S1 and S2), 25 km (station S3 and S4) and 70 km (station S5) (FIG. 1), using the representation theorem:

$$U_{station\ i}(t) \approx \sum_{S} G^{i}(x,y,t) * F_{M}\ (x,y,t) \qquad (4)$$

where * is the convolution operator. The summation over space integrates the contributions from the finite fault that has been discretized into a 2-D grid of subfaults. $F_M\ (x,y,t)$ is the slip rate function at position (x,y) computed using the source model defined above, while $G^i(x,y,t)$ represent the Green's functions calculated using the discrete wavenumber technique in the frequency range $0-5\ Hz$ [30], [31].

Finally, the PGA is computed using an orientation-independent measure proposed by [32] (GMRoTD50). This measure comprises a rotation of the two orthogonal components from 1 to 90, and evaluates PGA from the geometric mean of the rotated time series.

Figure APPENDIX 2 illustrates a realization of kinematic rupture from case 5 (TABLE 1), with the calculated accelerations for both the EW and the NS components (black and red solid lines, respectively). The far-field acceleration Equation (3) is also shown.

3.2.Computation of the PGA sensitivity

We consider 8 rupture scenarios, reported in TABLE 1. In order to consider potential variations of the PGA sensibility due to the hypocenter position, we implement 3 different locations of the hypocentre (along-strike coordinates of 20%, 50% and 80% of the rupture length). In addition, we generate 50 rupture realizations for each nucleation position, leading to 150 rupture realizations for each of the 8 scenarios. The first scenario (referred to as case

1) assumes $\mu_{Vr} = 3km/s$, $\sigma_D = 0.5\mu_D$ and $\sigma_{Vr} = 0.25\,\mu_{Vr}$. The correlation lengths in the along-strike and down-slip directions are derived from the $M_w - [a_x; a_z]$ scaling relationship found by [20]. The final slip and the rupture velocity are supposed to be uncorrelated ($\rho_{D\text{-}Vr}$=0) [15], while the final slip and the peak slip rate are assumed to be positively correlated ($\rho_{D\text{-}psv}$=0.8 [2]). Since such a positive correlation is found in most of the published studies (e.g. [33]), the value of $\rho_{D\text{-}psv}$=0.8 is kept for all the considered cases. The parameters of the reference case 1 are then perturbed independently to generate 7 additional cases of rupture scenarios. The sensitivities S_{PGA_k} to the different source parameters are then computed as:

$$S_{\mathrm{PGA}_k} = \frac{(\overline{\mathrm{PGA_k}} - \overline{\mathrm{PGA_r}})/\overline{\mathrm{PGA_r}}}{(P_\mathrm{k} - P_\mathrm{r})/P_\mathrm{r}} \tag{5}$$

Where $\overline{\mathrm{PGA_k}}$ and $\overline{\mathrm{PGA_r}}$ are the average PGA values computed for the case k and the reference case r, P_k and P_r are the values of the perturbed parameter for case k and r, respectively. Cases 2, 3, 4, 5 and 8 are associated to the sensitivity of μ_{Vr}, σ_D, σ_{Vr}, a_x and $\Delta\tau$, and are compared with the reference case r=1, while cases 6 and 7 are used to quantify the sensitivity of $\rho_{D\text{-}Vr}$ and are compared to reference case r=4.

FIG. 5 represents the PGA sensitivity to each source parameter for all the considered near-field stations as well as using the far-field approximation. The median sensitivity over the 150 rupture realizations is represented by coloured full circles, while the open black circles represent the 16% and 84% quantiles.

3.3.Results

We first consider the PGA sensitivity computed in the far-field approximation (FIG. 5). The first striking observation is that the PGA sensitivity is essentially controlled by the large-scale source parameters Vr and $\boldsymbol{\Delta\tau}$, and by the amplitude of the rupture velocity fluctuation σ_{Vr}. The PGA sensitivity to μ_{Vr} has the largest average value (1.4) and is the less variable (16% and 84% quantiles equal to 0.9 and 1.9, respectively). Besides, the PGA sensitivity to $\Delta\tau$ is more variable (16% and 84% quantiles equal to -0.4 and 0.9, respectively, with a mean value of 0.2. Note that this is much lower than the value of 0.8 expected from Equation (1). As explained in sections 2.3 the stopping phases generated by the rupture arrest at the fault boundaries in homogeneous ruptures are very poorly sensitive to the stress drop (the PGA sensitivity to $\Delta\tau$ is then ~0.1, see FIG. 2g). This suggests that the rupture arrest at the fault boundaries remains the main mechanism of PGA generation in our suite of heterogeneous ruptures. In this case, the choice of the tapering function used to avoid unphysical source parameters discontinuities at the fault boundaries may significantly impact the PGA value. By considering the suite of rupture model of case 1 as a reference, and by applying a 60%-

larger taper length on those models, we obtain a sensitivity value of -0.17. This show that the arbitrary choice of the tapering function may be a significant source of epistemic uncertainty in PGA computation based on kinematic source modelling.

In order to illustrate the variability of the PGA sensitivity to $\boldsymbol{\Delta\tau}$ in the far-field approximation, FIG. 6a and FIG. 6b represent 2 rupture realizations generated by resizing the rupture parameter distributions of FIG. 3a and FIG. 3b to obtain ruptures with a length of 55 km instead of 70 km (the along-strike grid size is scaled by 55/70 and the slip is scaled so to preserve the seismic moment). The comparison between FIG. 3a and FIG. 6a shows that a stress drop increase can attenuate a stopping phase and hence reduce the PGA, while FIG. 3b and FIG. 6b illustrate another mechanism, in which the stress drop increase changes the location of the PGA generation and induce a PGA increase. Furthermore, the average sensitivities to the statistical source parameters ($\sigma_D, \sigma_{Vr}, a_x,\ \rho^+, \rho^-$) range between -0.17 and 0.14. In addition to these smaller values, the ratios between the average absolute and the 68% confidence interval are also smaller, indicating that there are no clear tendencies.

The results obtained at the near-field stations also reveal a strong dominance of the average rupture velocity effect. The sensitivity values obtained at station S5, located at a R_{rup} distance equal to the rupture length, are very close to the value obtained in the far-field approximation, using Equation (3). We note, however, a stronger sensitivity to the rupture velocity at stations S2 and S4. This is because in case of a nucleation at the left or at the centre of the fault, strong directivity effects affect those stations. Note that we do not compute the PGA sensitivity to the stress drop, because it controls the fault dimension and hence modifies the position of the source heterogeneities with respect to the stations.

Furthermore, it is interesting to note that the average sensitivity to σ_{Vr} (amplitude of the rupture velocity fluctuation) is significant, ranging from ~0.3 to ~0.5 at stations S3, S4 and S5, while it remains close to 0 at station S1, with the 16% and 84% quantiles equal to -0.3 and 0.5, respectively). One explanation is that the PGA values at station S1 are essentially controlled by a small portion of the rupture area (statistically equally occupied by small or high rupture velocity patches), while the other stations, located at larger distances, “see” the whole rupture and PGA is then rather controlled by the maximum rupture velocity patches.

However, it is important to mention that the sensitivity alone is not sufficient to quantify the importance of a given source parameter, because each parameter has its own range of variability. Defining the physically possible range of source parameters is important. For example, analyses of past earthquake show that the rupture speed can vary between 0.6 and 0.85Vs [24], representing a potential ratio change of about 1.4. On the other hand, several studies report that the stress drop variability is well characterized by a log normal distribution with $\sigma_{\ln(\Delta\boldsymbol{\tau})} \approx 0.8$ (e.g. [4], [20], [34]), which means a potential factor change of 4.3 considering the 68% confident interval.

4. PGA variability

Using our synthetic ground motion database, we next compute the between-event variability of PGA, referred to as $\sigma_{\ln(PGA)}$. It is defined as the standard deviation of the natural logarithm PGA values, computed over 150 rupture realizations (50 realizations for each of the 3 nucleation positions). The values of $\sigma_{\ln(PGA)}$ for each station and for the 8 analysed cases are displayed in FIG. 7. First, we note that the $\sigma_{\ln(PGA)}$ values at station S5 and using the far-field approximation are slightly above the values reported in Ground Motion Predictions Equations (GMPEs) (ranging between 0.23 and 0.42 [8]), which are essentially derived from far-field recordings. The values obtained for the 8 cases are in overall similar for each case, meaning that the statistical source parameters have little impact on the PGA variability. We note, however, that $\sigma_{\ln(PGA)}$ generally has a smaller value for small values of the correlation lengths a_x and a_z (case 5). $\sigma_{\ln(PGA)}$ is also higher at the stations S2, S4, strongly affected by directivity effects, as the standard deviation of the rupture velocity increases (cases 4, 6 and 7). Finally, $\sigma_{\ln(PGA)}$ reaches its highest value (~0.6) at station S1, which is the closest to the rupture.

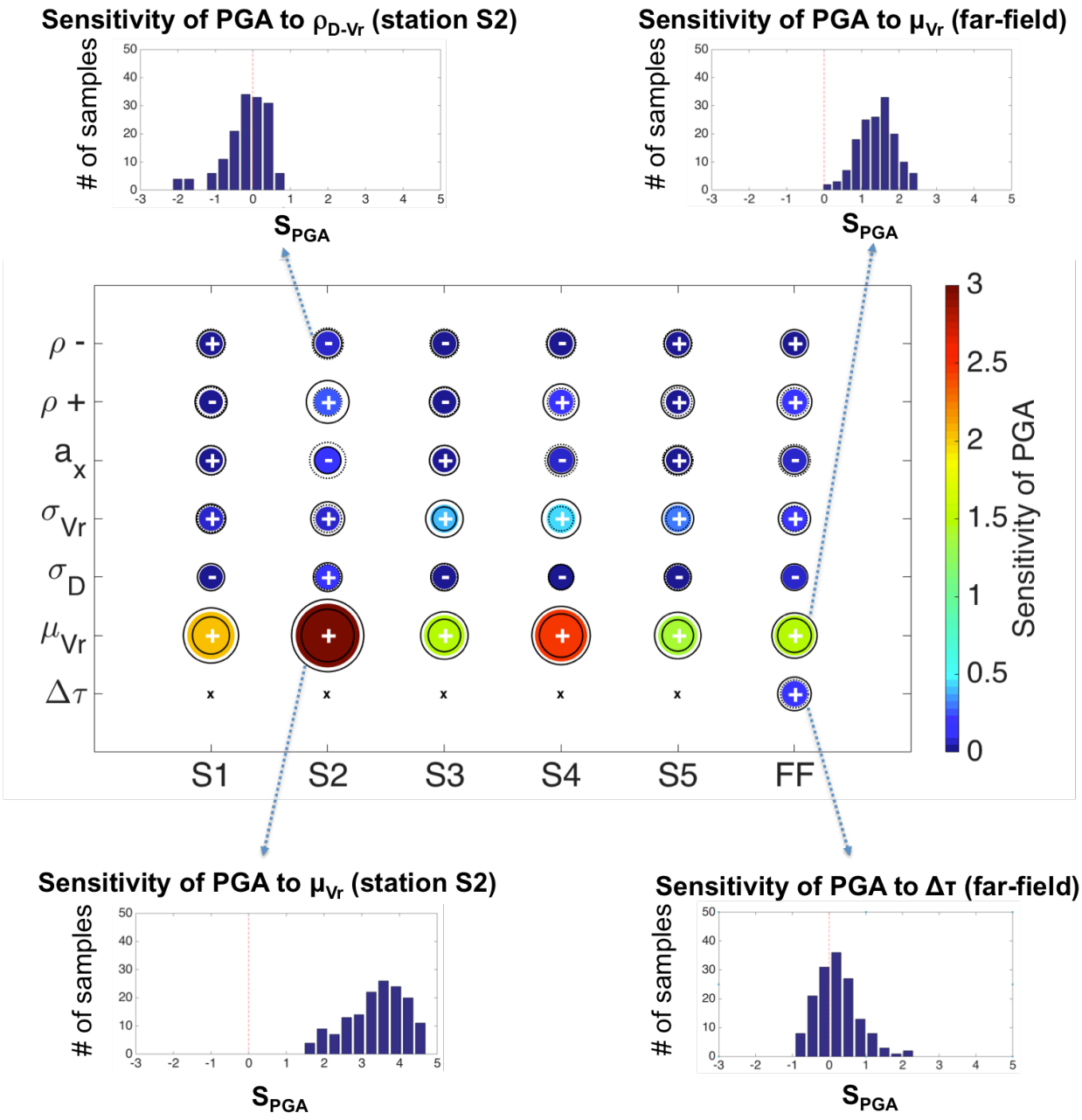

FIG. 5. Sensitivity of the PGA to the different kinematic rupture parameters at stations S1 to S5, as well as for the far-field approximation. The colors represent the median value of PGA computed for 150 simulations (50 realizations for the three considered hypocenter). The (+) and (-) represent the sign of the sensitivity median value. The contour lines represent the quantiles 16% and 84%, shown by solid lines if the values are positive, and by dashed lines for negative values. For illustration, 4 histograms of the sensibility values of the PGA are shown.

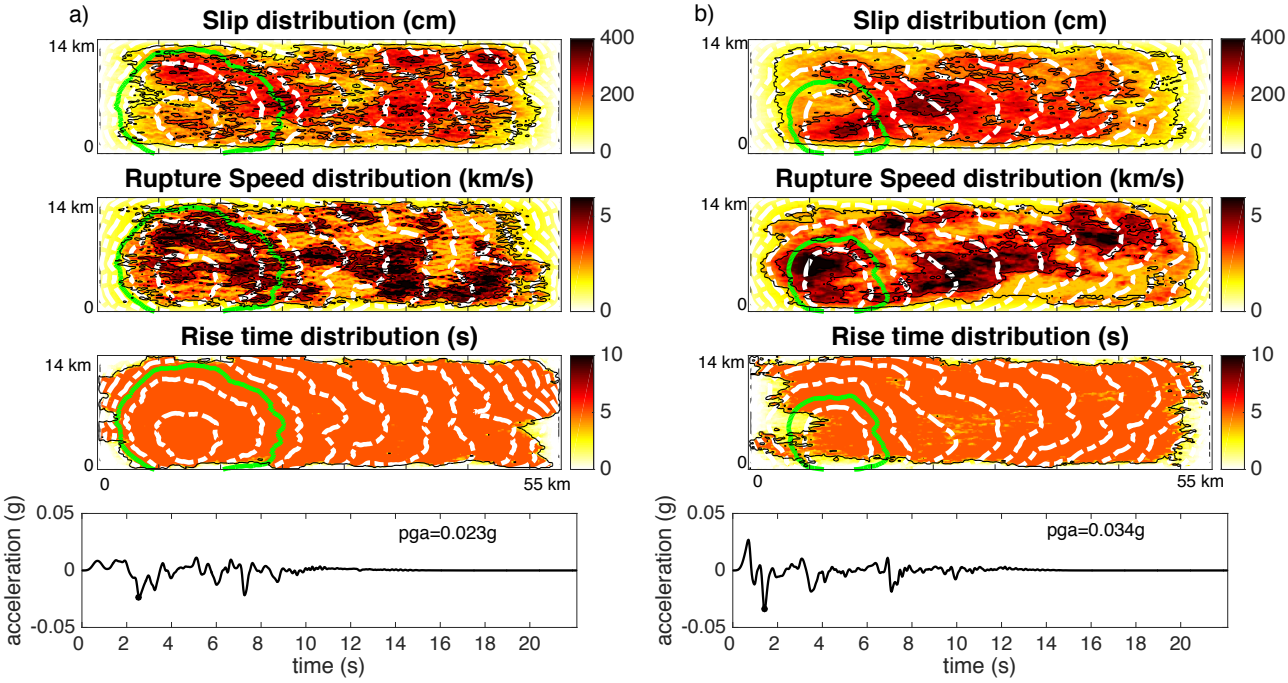

*FIG. 6. Two realizations of heterogeneous ruptures of a **M**7 event, with L=55km, V_r=3km/s, and T_{rise}=4s, tapered at the boundaries and the corresponding acceleration computed using Equation (3). The distribution of the slip, rupture speed and rise time are rescaled from FIG. 3.*

5. Conclusion

Deploying ground motion simulations based on kinematic rupture models, we investigate the origin of the PGA and its variability. We obtained the following results:

(1) in the case of homogeneous ruptures, the PGA is essentially controlled by the rupture stopping phases at the fault border. Those phases are poorly sensitive to the stress drop but very sensitive to the rupture velocity value and the tapering function used to avoid stress singularities at the fault borders;

(2) in the case of heterogeneous ruptures, the PGA is mainly controlled by the average rupture velocity and to a lesser extent, by the average stress drop and the standard deviation of rupture velocity (controlling the amplitude of rupture velocity fluctuations). The other statistical source parameters (correlation length and correlation between slip and rupture velocity) have a very weak impact on the PGA;

(3) the sensitivity to the stress drop is ~0.2, that is much smaller than the value of 0.8 predicted by the random vibration theory and assuming a Brune (1970) source model;

(4) the PGA variability $\sigma_{\ln(PGA)}$ increases as the distance to the rupture R_{rup} decreases. It is slightly larger than the reported between-event variabilities at distances of the order of the rupture dimension, and reaches 0.6 for R_{rup} = 5 km.

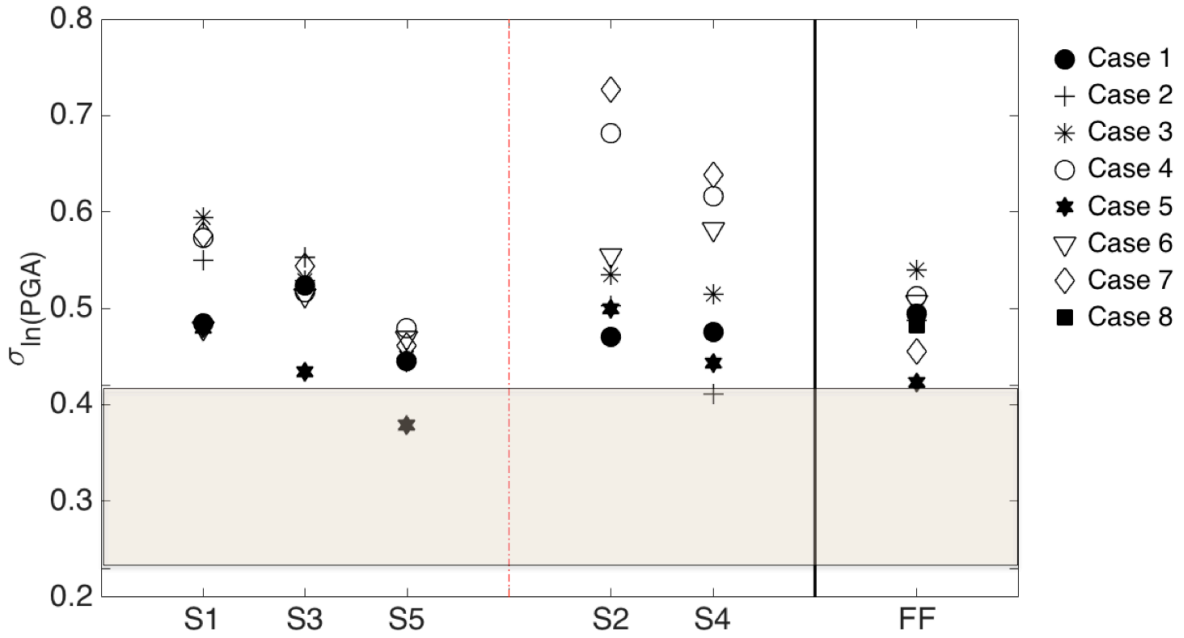

FIG. 7. PGA variability for the different cases defined in TABLE 1 and for the different stations. The grey box delimits the values of the between-event variability obtained in some recent GMPEs [8].

APPENDIX

APPENDIX 1: 1-D velocity model used in our simulations.

H (km)	Vp (km/s)	Vs (km/s)	Rho (g/cm^3)	Q_s
0.00	6.20	3.58	2.70	220
14.00	6.80	3.93	2.86	220
34.00	8.05	4.65	3.28	220
50.00	8.25	4.76	3.29	220
80.00	8.50	4.91	3.50	220

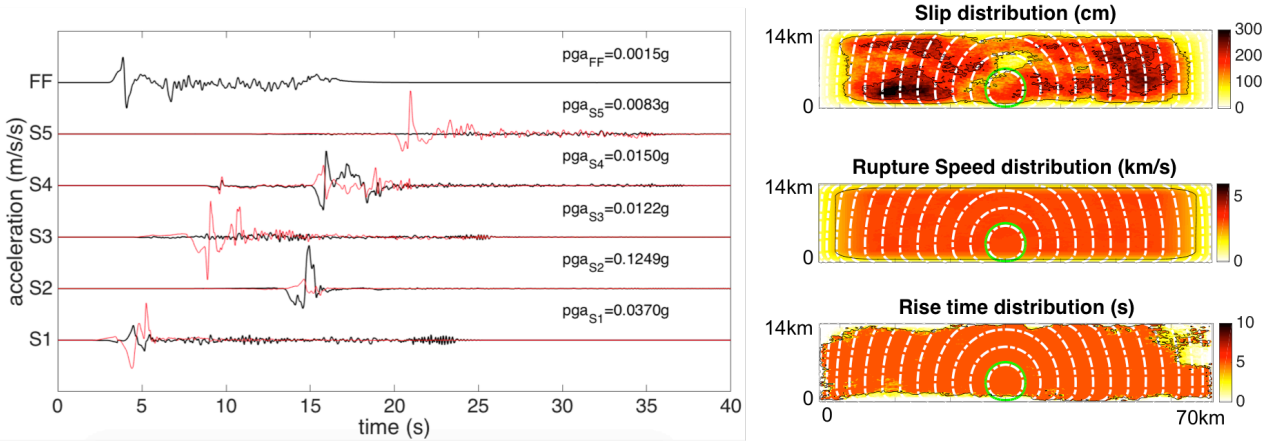

APPENDIX 2: Accelerograms computed at different stations with the horizontal components in black (EW) and red (NS), as well as in the far-field (FF) approximation, resulting from the rupture realization shown on the right, corresponding to case6 of TABLE 1.

REFERENCES

[1] M. P. Moschetti, S. Hartzell, L. Ramírez-Guzmán, A. D. Frankel, S. J. Angster, and W. J. Stephenson, "3D Ground-Motion Simulations of Mw 7 Earthquakes on the Salt Lake City Segment of the Wasatch Fault Zone: Variability of Long-Period (T≥1 s) Ground Motions and Sensitivity to Kinematic Rupture Parameters," *Bull. Seismol. Soc. Am.*, Jun. 2017.

[2] S. G. Song, L. A. Dalguer, and P. M. Mai, "Pseudo-dynamic source modelling with 1-point and 2-point statistics of earthquake source parameters," *Geophys. J. Int.*, vol. 196, no. 3, pp. 1770–1786, Mar. 2014.

[3] D. Bindi, D. Spallarossa, and F. Pacor, "Between-event and between-station variability observed in the Fourier and response spectra domains: comparison with seismological models," *Geophys. J. Int.*, vol. 210, no. 2, pp. 1092–1104, Aug. 2017.

[4] F. Cotton, R. J. Archuleta, and M. Causse, "What is Sigma of the Stress Drop?," *Seismol. Res. Lett.*, vol. 84, no. 1, pp. 42–48, Jan. 2013.

[5] A. Oth, H. Miyake, and D. Bindi, "On the relation of earthquake stress drop and ground motion variability," *J. Geophys. Res. Solid Earth*, vol. 122, no. 7, p. 2017JB014026, Jul. 2017.

[6] J. N. Brune, "Tectonic stress and the spectra of seismic shear waves from earthquakes," *J. Geophys. Res.*, vol. 75, no. 26, pp. 4997–5009, Sep. 1970.
[7] D. M. Boore, "Stochastic simulation of high-frequency ground motions based on seismological models of the radiated spectra," *Bull. Seismol. Soc. Am.*, vol. 73, no. 6A, pp. 1865–1894, Dec. 1983.
[8] M. Causse and S. G. Song, "Are stress drop and rupture velocity of earthquakes independent? Insight from observed ground motion variability," *Geophys. Res. Lett.*, vol. 42, no. 18, p. 7383, Sep. 2015.
[9] R. J. Archuleta and C. Ji, "Moment rate scaling for earthquakes 3.3 ≤ M ≤ 5.3 with implications for stress drop," *Geophys. Res. Lett.*, vol. 43, no. 23, p. 12,004–12,011, 2016.
[10] R. Madariaga, *High frequency radiation from crack (stress drop) model of earthquake faulting*, vol. 51. 1977.
[11] M. Vallée and C. Satriano, "Ten year recurrence time between two major earthquakes affecting the same fault segment," *Geophys. Res. Lett.*, vol. 41, no. 7, pp. 2312–2318, Apr. 2014.
[12] M. Causse, F. Cotton, and P. M. Mai, "Constraining the roughness degree of slip heterogeneity," *J. Geophys. Res.*, vol. 115, no. B5, p. @CitationB05304-@CitationB05304, Jan. 2010.
[13] J. G. F. Crempien and R. J. Archuleta, "Within-Event and Between-Events Ground Motion Variability from Earthquake Rupture Scenarios," *Pure Appl. Geophys.*, vol. 174, no. 9, pp. 3451–3465, Sep. 2017.
[14] I. A. Beresnev, "Factors controlling high-frequency radiation from extended ruptures," *J. Seismol.*, vol. 21, no. 5, pp. 1277–1284, Sep. 2017.
[15] J. Schmedes, R. J. Archuleta, and D. Lavallee, "Correlation of earthquake source parameters inferred from dynamic rupture simulations (English)," *J Geophys Res*, vol. 115, no. B3, cover date 2010.
[16] S. G. Song, "Developing a generalized pseudo-dynamic source model of Mw 6.5–7.0 to simulate strong ground motions," *Geophys. J. Int.*, vol. 204, no. 2, pp. 1254–1265, Feb. 2016.
[17] S. G. Song, "The effect of fracture energy on earthquake source correlation statistics," *Bull. Seismol. Soc. Am.*, vol. 105, no. 2A, pp. 1042–1048, Apr. 2015.
[18] P. Liu, R. J. Archuleta, and S. H. Hartzell, "Prediction of broadband ground-motion time histories; hybrid low/high- frequency method with correlated random source parameters," *Bull. Seismol. Soc. Am.*, vol. 96, no. 6, pp. 2118–2130, Dec. 2006.
[19] E. Tinti, E. Fukuyama, A. Piatanesi, and M. Cocco, "A kinematic source-time function compatible with earthquake dynamics," *Bull. Seismol. Soc. Am.*, vol. 95, no. 4, pp. 1211–1223, Aug. 2005.
[20] P. M. Mai and G. C. Beroza, "A spatial random field model to characterize complexity in earthquake slip," *J. Geophys. Res.*, vol. 107, no. B11, Nov. 2002.
[21] B. C. Papazachos, E. Scordilis, D. Panagiotopoulos, C. Papazachos, and G. Karakaisis, "Global relations between seismic fault parameters and moment magnitude of earthquakes," *Bull. Geol. Soc. Greece*, vol. 36, pp. 1482–1489, Jan. 2004.
[22] A. F. McGarr and J. B. Fletcher, "Maximum slip in earthquake fault zones, apparent stress, and stick-slip friction," *Bull. Seismol. Soc. Am.*, vol. 93, no. 6, pp. 2355–2362, Dec. 2003.
[23] H. Kanamori and D. L. Anderson, "Theoretical basis of some empirical relations in seismology," *Bull. Seismol. Soc. Am.*, vol. 65, no. 5, pp. 1073–1095, Oct. 1975.
[24] T. H. Heaton, "Evidence for and implications of self-healing pulses of slip in earthquake rupture," *Phys. Earth Planet. Inter.*, vol. 64, no. 1, pp. 1–20, Nov. 1990.
[25] P. M. Mai, P. Spudich, and J. Boatwright, "Hypocenter Locations in Finite-Source Rupture Models," *Bull. Seismol. Soc. Am.*, vol. 95, no. 3, pp. 965–980, Jun. 2005.
[26] D. M. Boore and J. Boatwright, "Average body-wave radiation coefficients," *Bull. Seismol. Soc. Am.*, vol. 74, no. 5, pp. 1615–1621, Oct. 1984.

[27] J. G. Heacock, U. S. O. of N. Research, and C. S. of Mines, *The Earth's Crust: Its Nature and Physical Properties*. American Geophysical Union, 1977.

[28] S. Latour, M. Campillo, C. Voisin, I. R. Ionescu, J. Schmedes, and D. Lavallée, "Effective friction law for small-scale fault heterogeneity in 3D dynamic rupture," *J. Geophys. Res. Solid Earth*, vol. 116, no. B10, p. B10306, Oct. 2011.

[29] P. Spudich and E. Cranswick, "Direct observation of rupture propagation during the 1979 Imperial Valley earthquake using a short baseline accelerometer array," *Bull. Seismol. Soc. Am.*, vol. 74, no. 6, pp. 2083–2114, Dec. 1984.

[30] M. Bouchon, "A simple method to calculate Green's functions for elastic layered media," *Bull. Seismol. Soc. Am.*, vol. 71, no. 4, pp. 959–971, Aug. 1981.

[31] F. Cotton and O. Coutant, "Dynamic stress variations due to shear faults in a plane-layered medium," *Geophys. J. Int.*, vol. 128, no. 3, pp. 676–688, Mar. 1997.

[32] D. M. Boore, J. Watson-Lamprey, and N. Abrahamson, "Orientation-Independent Measures of Ground Motion," *Bull. Seismol. Soc. Am.*, vol. 96, no. 4A, pp. 1502–1511, Aug. 2006.

[33] S. G. Song, A. Pitarka, and P. Somerville, "Exploring Spatial Coherence between Earthquake Source Parameters," *Bull. Seismol. Soc. Am.*, vol. 99, no. 4, pp. 2564–2571, Aug. 2009.

[34] F. Courboulex, M. Vallée, M. Causse, and A. Chounet, "Stress-Drop Variability of Shallow Earthquakes Extracted from a Global Database of Source Time Functions," *Seismol. Res. Lett.*, vol. 87, no. 4, pp. 912–918, Jul. 2016.